12th International Symposium on Turbulence and Shear Flow Phenomena (TSFP12)
Osaka, Japan, July 19–22, 2022

ENERGY EXCHANGES IN THE WAKE OF A MULTISCALE SYSTEM

Neelakash Biswas
Department of Aeronautics
Imperial College London, UK
n.biswas20@imperial.ac.uk

Oliver R.H. Buxton
Department of Aeronautics
Imperial College London, UK
o.buxton@imperial.ac.uk

ABSTRACT

In this study, we investigate the energy exchanges between coherent structures in the wake of a model multiscale geometry consisting of a cylinder and a leeward control rod using Particle Image Velocimetry (PIV) data. For certain control rod positions, we observe new secondary coherent motions with distinct characteristic frequencies in the flow field aside from the frequencies associated with the sheddings of the control rod, the main cylinder and its harmonics. We employ the multiscale triple-decomposition technique proposed by Baj *et al.* (2015), to extract the spatio-temporal structure of the coherent modes associated with each of the frequencies and also study the energy exchanges to/from the coherent motions using the triple decomposed kinetic energy budget equations derived by Baj & Buxton (2017). We find almost the same sequence of energy transfers between the primary and secondary modes as reported by Baj & Buxton (2017) for a different multiscale geometry, hinting at a possible universality of these structures in any multiscale flow. We perform a series of PIV experiments to look for similar energy exchanges in the wake of a representative rotor which is also a multiscale system due to the presence of multiple length (and time) scales simultaneously introduced in the flow from the nacelle, tower and rotor blades. If the universality in energy exchanges is upheld even for a multiscale system with rotation, it would prove to be a powerful tool for the near wake-modeling of wind turbines.

INTRODUCTION

Multiscale flows are encountered everywhere around us, for instance flow through offshore platforms, a forest or cityscape or even flow through a wind turbine. In any multiscale flow different length (and time) scales are simultaneously introduced into the flow. Understanding the multiscale interactions in these flows is not only of fundamental interest but also is important in modelling industrially relevant flows such as the wake of a wind turbine. In a wind turbine wake, forcings are introduced at different length scales by the tower, nacelle, tip vortices etc. The importance of the nacelle and tower in the development of the near wake has been highlighted in some studies e.g. (Foti *et al.*, 2018), but has not been quantified in detail. Understanding the energy exchanges in such a complex multiscale geomerty requires prior understanding from a simpler multiscale flow. Hence, we first discuss results of a simplified multiscale geometry consisting of a main cylinder and a leeward control rod. The control rod has a diameter an order of magnitude smaller than the main cylinder, thereby coherence is introduced into the flow at significantly different length and time scales. Interestingly, for certain positions of the control rod, the interaction between the wakes of the two wake generating bodies generates new coherent structures. In fact, Cicolin *et al.* (2021) recently reported the observation of two such new frequencies which exactly corresponded to the sum and difference of the frequencies corresponding to the fundamental sheddings of the control rod and the main cylinder. In this work, we develop a deeper understanding of the process of generation of these new coherent motions with the same data set as Cicolin *et al.* (2021). In order to understand the interaction between the different coherent structures, we employ the multiscale triple decomposition technique proposed by Baj *et al.* (2015) where the flow field is decomposed as the combination of the mean component ($\bar{u}$), sum of contributions from different coherent motions ($\sum_l \tilde{u}_l$) and the incoherent or stochastic part (u') as follows

$$u(x,y,t) = \bar{u}(x,y) + \sum_l \tilde{u}_l(x,y,t) + u^{'}(x,y,t) \tag{1}$$

In order to obtain the energy transfers to/from the coherent structures, we use the multiscale triple decomposed turbulent kinetic energy transport equations derived by Baj & Buxton (2017). Based on the coherent energy budget equations, we identify the differences in the process of formation of different coherent structures and also their roles in the energy cascade process. Finally, some preliminary results from PIV experiments on a model wind turbine is shown and the multiscale nature of the wind turbine wake is discussed.

PIV experiments and data set

The PIV experiments of Cicolin *et al.* (2021) had a main cylinder of diameter (D) 0.05m and the control rod's diameter (d) was $0.1D$. The control rod was mounted at a centre-to-centre distance (R) of $0.7D$ while the control rod angle (θ) was varied between 90° and 140° (see fig. 1). The free stream

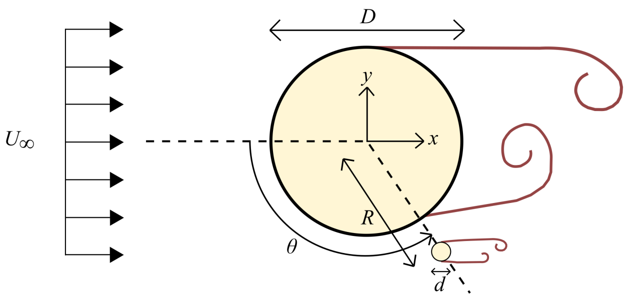

Figure 1. A schematic of the multiscale geometry consisting of a main cylinder and a control rod (the image is reproduced from Biswas *et al.* (2022))

velocity (U_∞) was fixed at 0.4m/s giving a Reynolds number $Re_D = 20 \times 10^3$ for the cylinder and $Re_d = 2 \times 10^3$ for the control rod. Readers are referred to Cicolin *et al.* (2021) for further details of the experimental measurements.

New PIV experiments are conducted on a scaled wind turbine model in the recirculating water channel in the hydrodynamics flume at Imperial College London. The 3D printed model wind turbine consisted of a nacelle and a tower to replicate the wake dynamics of an actual wind turbine to the extent possible. Fig. 2 shows a schematic of the model geometry along with important dimensions. The turbine is run by a stepper motor RS 829-3512 and the torque is transmitted to the shaft connected to the wind turbine through a pulley and belt mechanism, that passes through the wind turbine tower. The freestream velocity was fixed to 0.2 m/s and maximum chord based Re was 4×10^3. Experiments were conducted at tip speed ratios (λ) varying from 3-6. 3 experiments were conducted over a large field of view (FOV) in the central cross sectional plane extending up to 3.5 rotor diameters in the streamwise direction. 3 Phantom v641 cameras were used to capture the data at a frequency of $100Hz$. The FOV of the first experiment (henceforth referred to as FOV 1) focused the region below the nacelle (see fig. 2) (a)) to capture the evolution of the tip vortices. In the second experiment, the FOV (FOV 2) focused the region above the nacelle to understand the effect of the tower. The third experiment focused on the nacelle wake. In this paper, preliminary results are shown for λ = 4.5 only in FOV 1 and FOV 2.

RESULTS AND DISCUSSIONS

By definition, a multiscale flow contains coherent motions of several distinct frequencies. To identify the important frequencies in the flow consisting of a main cylinder and a control rod considered herein, let us first observe the evolution of the transverse velocity spectra for different values of θ with streamwise distance. In fig. 3(a) see that the near field ($x/D =$ 1) for $\theta = 90°$ consists of a number of prominent frequencies. The low frequency peak at Strouhal number ($S_t = fD/U_\infty$) of around 0.166 (associated frequency, $f_m \approx 1.3Hz$) corresponds to the vortex shedding of the main cylinder, while the other strong peak at $S_t = 2.45$ (associated frequency, $f_c \approx 19.6Hz$) corresponds to the fundamental shedding mode of the control rod. Around f_c, two additional prominent peaks are observed (indicated by green arrows) which correspond to the frequencies $f_c \pm f_m$. At $x/D = 2$, f_m is more energetic and harmonics of f_m are observed. However, f_c and $f_c \pm f_m$ are not observed at this station, which shows that these modes are spatially less persistent. The strength of f_c as well as $f_c \pm f_m$ depends on the

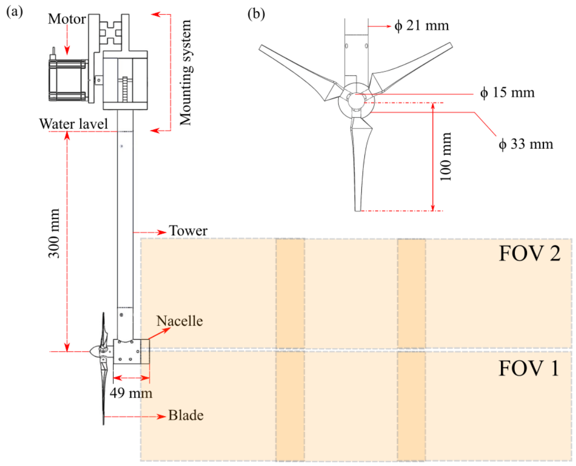

Figure 2. (a) Side view wind turbine model along with motor and mounting system. The field of view of the two experiments are shown as FOV 1 and FOV 2. Sub figure (b) shows the front view of the wind turbine model.

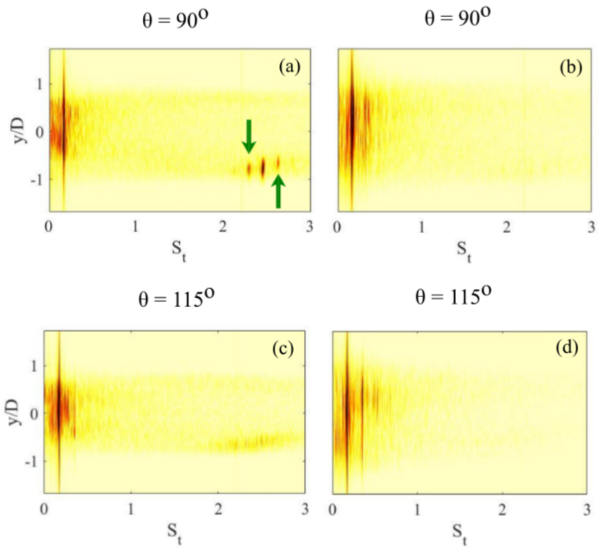

Figure 3. Frequency spectra of the transverse component of the fluctuating velocity at $x/D = 1$ (a,c) and $x/D = 2$ (b,d) for $\theta = 90°$ and $\theta = 115°$

precise position of the control rod. At $\theta = 115°$, the control rod is effectively shadowed by the separated shear layer from the main cylinder, hence f_c is not prominent, nor are $f_c \pm f_m$ (see fig. 3(c)), while the harmonics of f_m are prominent at $x/D = 2$ (fig.3(d)). Interestingly fig. 3(a) reveals a particular spatial configuration of the modes $f_c \pm f_m$. $f_c + f_m$ resides near the separated shear layer between the main cylinder and the control rod whereas, $f_c - f_m$ resides more towards the opposite separated shear layer of the control rod, which is remarkably similar to the observation of Baj & Buxton (2017) for a fundamentally different multiscale flow, a one dimensional multiscale static mixer.

The spatio-temporal velocity field ($\tilde{u}_l(x,y)$) associated with each of the frequencies identified in the flow field can be obtained by using the multi-scale triple decomposition shown in equation 1. We apply optimal mode decomposition (OMD), first proposed by Wynn *et al.* (2013) to obtain ($\tilde{u}_l(x,y)$) for each of the coherent motions. The OMD algorithm is a generalised version of the dynamic mode decomposition (DMD) algorithm proposed by Schmid (2010) and can identify individual coherent motions in the flow field under investigation. We apply the multiscale triple decomposition on the data set and show the modes associated with f_c, f_m and $f_c \pm f_m$ for $\theta = 90^\circ$ in fig. 4. The filled contours show the time averaged kinetic energies (defined as $\frac{1}{2}(\overline{\tilde{u}_l \tilde{u}_l + \tilde{v}_l \tilde{v}_l})$) of the modes, while the contour lines represent the iso-phase lines of transverse velocity component obtained from the complex OMD modes (see Biswas *et al.* (2022) for more details). Fig. 4(a) and (b) show the modes corresponding to the shedding of the control rod and main cylinder respectively, which is evident by the presence of a phase correlated region behind the respective wake generating bodies in which the kinetic energies associated with the modes are concentrated. The location where the kinetic energy of the individual modes attain maximum is shown by a '+' sign. The modes corresponding to the harmonics of the main cylinder's shedding frequency were also captured through OMD, but not shown here (see Biswas *et al.* (2022) for details).

The secondary modes however are not captured by the OMD spectrum even when the rank of the projection/dynamic matrices was set to very high values while performing the analysis. However, since we have the phase reference of the secondary modes, *i.e.* $f_c \pm f_m$, we can use phase averaging (see for instance Reynolds & Hussain (1972); Cantwell & Coles (1983)) to extract the modes associated with the secondary frequencies observed in fig. 3(a). Subsequently, we take the second Fourier mode of the phase-averaged flow field in order to produce a complex spatial mode that mimics the OMD modes. We encourage readers to refer to Baj & Buxton (2017) for an extensive description of identification of the secondary modes using phase averaging. The secondary modes shown in fig. 4(c-d) show a significantly large phase-correlated region in the vicinity of the control rod. Note that the presence of a phase correlated region of velocity (vorticity) correlates well with the definition of a coherent structure proposed by Hussain (1986). For the lower secondary mode ($f_c - f_m$) in fig. 4(c), most of the energy of the mode is located towards the lower shear layer of the control rod, while for the higher secondary mode ($f_c + f_m$) in fig. 4(d), it is located more towards the separated shear layer between the main cylinder and the control rod. This spatial configuration of the secondary modes is the same as that observed in the frequency spectra in fig. 3(a). The kinetic energy of the secondary modes peaks further downstream compared to the control rod's fundamental shedding mode for which the peak was located very close to the control rod. This difference in the location of peak kinetic energy was also noted by Baj & Buxton (2017) and it hints at the fact that a different mechanism is involved behind the formation of the secondary modes.

In order to understand the process of generation of these modes, it is important to track the energy transfers to/from the individual coherent modes and the mean flow. Similar to the kinetic energy budget equations for the mean flow, Baj & Buxton (2017) derived separate kinetic energy budget equations for each of the coherent modes present in a multiscale flow using the multiscale triple decomposition shown in equation 1. The coherent energy budget equation is expressed in symbolic terms as

$$\frac{\partial \tilde{k}_l}{\partial t} = -\tilde{C}_l + \tilde{P}_l - \hat{P}_l + \left(\tilde{T}_l^{+} - \tilde{T}_l^{-}\right) - \tilde{\varepsilon}_l + \tilde{D}_l \qquad (2)$$

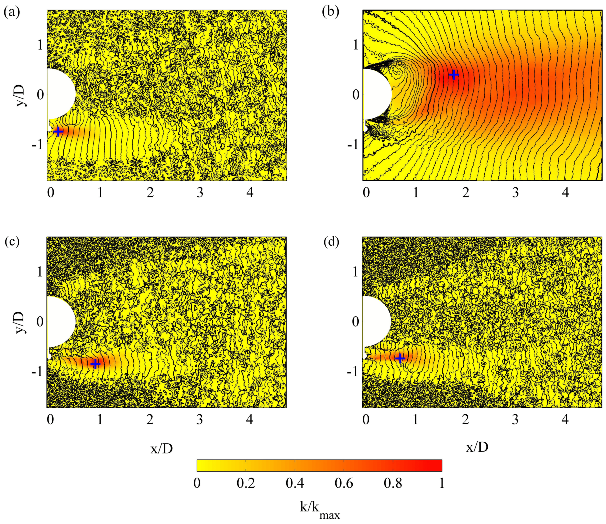

Figure 4. Energy and iso-phase lines associated with (a) control rod's shedding mode (f_c), and (b) main cylinder's shedding mode (f_m). The contour lines are shown from $-\pi$ to π at step size $\pi/2$ in (a) and $\pi/15$ in (b). The corresponding modes for the low and high frequency secondary modes ($f_c + f_m$) are shown in fig. (c) and (d) respectively. The contour lines are shown between $-\pi$ to π at a step size of $\pi/2$ for both the secondary modes. The '+' sign shows the location where kinetic energy is maximum.

In equation 2, the term on the left hand side corresponds to the unsteady term, whilst the sources/sinks are arranged on the right hand side. The term $-\bar{C}_l$ is the convection term and $\tilde{P}_l$ denotes the coherent energy production term (from the mean flow). Here, $\tilde{P}_l$ is defined as $-\sum_{f_s} \overline{\tilde{u}_i^{f_s} \tilde{u}_j^{f_l} \frac{\partial \bar{u}_i}{\partial x_j}}$, where s can be any coherent motion including the l^{th} coherent motion. The terms $\hat{P}_l$, ε_l and D_l represent the production of stochastic turbulent kinetic energy from the l_{th} coherent motion, dissipation and diffusion terms respectively. The term denoted as $\tilde{T}_l^{+} - \tilde{T}_l^{-}$ is the nonlinear triadic energy transfer term and accounts for the net non-linear triadic energy transfer to/from the l_{th} coherent mode from/to the other coherent modes. The terms is defined as

$$\tilde{T}_l^{+} - \tilde{T}_l^{-} = -\frac{1}{2} \sum_{f_s, f_t} \overline{u_i^{f_l} u_j^{f_t} \frac{\partial u_i^{f_s}}{\partial x_j}} + \frac{1}{2} \sum_{f_s, f_t} \overline{u_i^{f_s} u_j^{f_t} \frac{\partial u_i^{f_l}}{\partial x_j}}. \qquad (3)$$

Here, the frequencies f_s and f_t correspond to other frequencies which might influence the non-linear energy gain/loss of f_l. (Baj & Buxton, 2017) argued that this term could be non-negligible only when the coherent structures involved in the energy exchange process formed a triad, i.e. $f_l \pm f_s \pm f_t = 0$.

Keeping this background in mind, let us now investigate the energy budget terms for the coherent modes observed in fig. 3(a) for $\theta = 90^\circ$ and try to understand their dynamics. Instead of reporting local profiles of the different kinetic energy budget terms at different streamwise stations, we obtain $\int_y ED/U_\infty dy$, where E is any kinetic energy budget term and show its evolution with streamwise distance. See that for f_m and f_c (fig. 5(a) and (b)), the main source term is the coherent energy production ($\tilde{P}_l$) compared to which the contribution

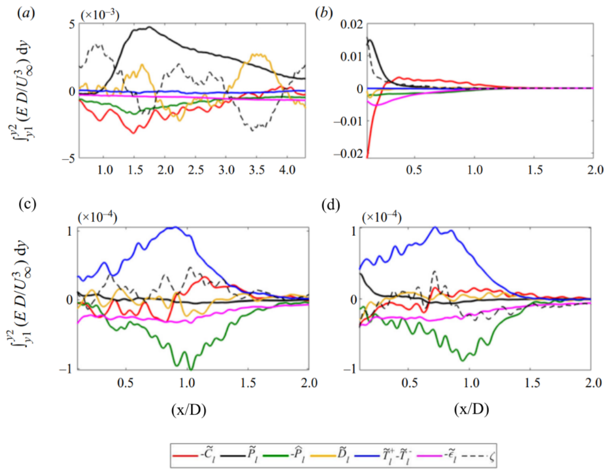

Figure 5. Streamwise evolution of the kinetic energy budget terms for (a) the main cylinder's and (b) the control rod's fundamental shedding modes at $\theta = 90°$. Sub figure (c) and (d) shows the same for the low and high frequency secondray modes respectively for $\theta = 90°$. The horizontal (– · –) line shows the 0 level for a reference.

of the $\tilde{T}_l^+ - \tilde{T}_l^-$ term is negligible. For $f_c \pm f_m$ (fig. 5(c,d)), the $\tilde{P}_l$ term is negligible and the major source of energy is the $\tilde{T}_l^+ - \tilde{T}_l^-$ term, which shows that $f_c \pm f_m$ are fundamentally different from either f_c and f_m. As these modes are not directly energised by the mean flow, it is imperative to term them as 'secondary modes' as opposed to f_c and f_m which are the 'primary modes'. The energy budget of the harmonics of f_m are not shown here for brevity. However, it is worthwhile to note that the harmonics of f_m behave in a mixed fashion, *i.e.* the energy transfer through $\tilde{P}_l$ and the $\tilde{T}_l^+ - \tilde{T}_l^-$ term are of similar magnitude for them (see Biswas *et al.* (2022) for details). The entire energy exchange process is illustrated through a flow diagram in fig. 6. The different coherent structures are represented as circles and placed in ascending order of their frequency. The net energy transfer to the modes from the mean flow is shown by thick arrows while the thin arrows represent non-linear energy transfers between different coherent modes. Note that the main source of non-linear energy gain of the two secondary modes is the high frequency primary mode (f_c). $f_c + f_m$ gives away some of its energy to f_m, while almost a similar amount of energy is transferred to $f_c - f_m$ from f_m. These energy exchanges are similar to the findings of Baj & Buxton (2017). Also, note that alongside the conventional energy cascade from large to small scales, there is a significant amount reverse energy cascade present.

This analysis on a rather simple multiscale geometry lays the foundation to understand more complicated industrially relevant flows such as the wake of a wind turbine. The wake of a wind turbine is inherently multiscale due to the forcing introduced at different length and time scales. For instance, the nacelle, tower and vortices shed from the rotor blade can have distinct characteristic frequencies and hence a distinct spatio-temporal coherent mode associated with each frequency as shown for the flow past a main cylinder and a control rod. It is possible that these new frequencies can interact with each other leading to new frequencies which can have significant impact on the evolution of the turbine wake. We show an instantaneous non-dimensional vorticity field of a wind turbine wake in fig. 7. FOV1 and FOV2 are obtained from different experiments and are stitched together to aid visual representa-

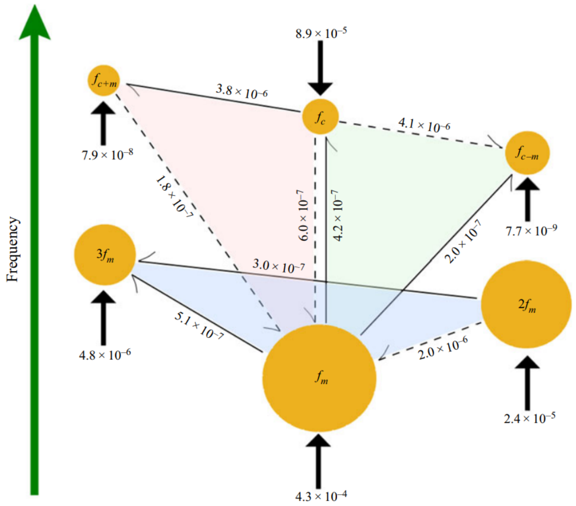

Figure 6. Combined schematic energy transfer diagram for the different modes identified within the flow. The modes are arranged such that characteristic frequency of the modes increases from bottom to top. The thick full headed arrows show the net energy transfer between the various modes and the mean flow. The single headed arrows show the non-linear triadic energy transfer between two modes. A solid line shows non-linear energy transfer from low-frequency to high-frequency, whilst the dashed lines show energy transfers from high-frequency to low-frequency - an inverse cascade.

tion. It can be seen that the near field of the turbine wake is rich with coherent structures and flow field is inherently complex. In FOV 1, the array of the tip vortices can be seen. The vortices shed from the 3 blades start interacting at a streamwise distance around $x/D = 2$ and merge into a single structure. In FOV 2, on the other hand, the presence of the tower causes the tip vortices to break down. Note that the vorticity levels in FOV 2 are significantly enhanced compared to FOV 1 and the tower acts as an important source for this asymmetry in the flow. We next characterise the frequency content in the flow. In fig. 8 fast Fourier transforms are evaluated at selected points based on the fluctuating transverse velocity component. The Strouhal number is calculated based on turbine diameter (0.2m) and freestream velocity (0.2m/s). For the present case, the numerical value of the Strouhal number is same as that of the frequency. At $x/D = 0.5$, $y/D = -0.5$ (fig. 8(a)), The dominant frequency is the blade frequency, $4.22Hz$. The harmonics of the blade frequency are also observed at this location. Further downstream at $x/D = 3$, $y/D = -0.5$ (fig. 8(c)), the dominant frequencies are the rotor frequency ($1.41Hz$) and its harmonics which correlates well with the merging of the tip vortices also seen in fig. 7. Interestingly, in fig. 8(c), apart from the blade/rotor frequency and their harmonics, some new frequencies are also observed. Fig. 8(b) shows the frequency spectrum near the nacelle shear layer at $x/D = 0.5$, $y/D = -0.1$. Here the dominant frequency is found to be around $0.71Hz$. If we non-dimensionalise this frequency based on the diameter of the nacelle, the Strouhal number comes out to be approximately 0.11. This Strouhal number correlates well with that reported for azimuthal shedding modes of an axisymmetric bluff body (Rigas *et al.*, 2014). Interestingly, at $x/D = 3$, $y/D = -0.1$, a low frequency dominant mode is observed at around $S_t = 0.27$. This frequency correlates well with the wake meandering frequencies reported in previous studies (Okulov *et al.*, 2014; Chamorro & Porté-

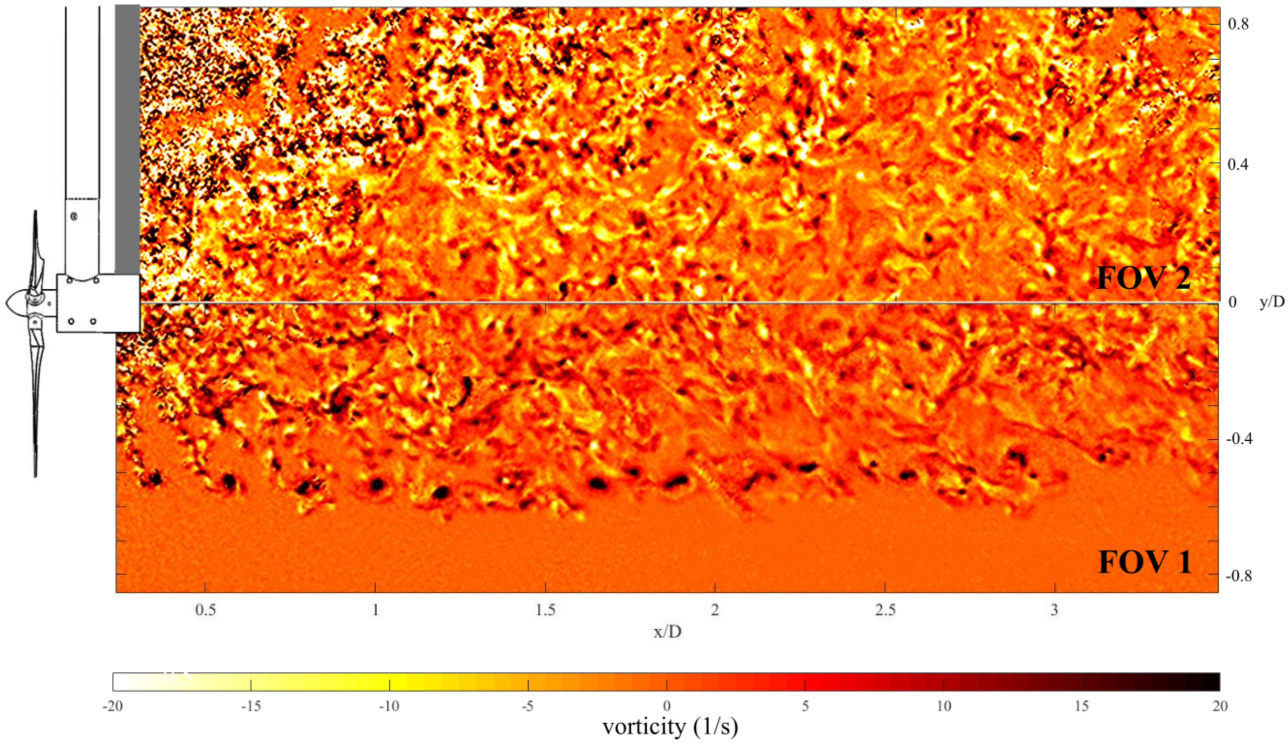

Figure 7. Instantaneous vorticity field of a wind turbine wake. FOV 1 and FOV 2 correspond to different experiments. They are stitched together for a visual representation of the entire wake.

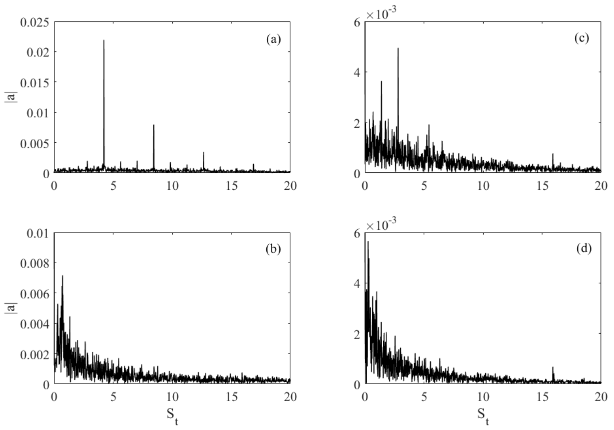

Figure 8. Transverse velocity spectra obtained at (a) $x/D = 0.5$, $y/D = -0.5$, (b) $x/D = 0.5$, $y/D = -0.1$ (c) $x/D = 3$, $y/D = -0.5$, and (d) $x/D = 3$, $y/D = -0.1$.

Agel, 2009). Apart from this frequency, a number of new non-dominant frequencies are also observed at this station which deserves further investigation.

CONCLUSIONS AND FUTURE WORK

In this paper we investigated the energy exchanges taking place between different coherent motions present in a multi-scale flow. The simplified multiscale system considered here consists of a cylinder and a control rod and contained new secondary frequencies that showed remarkable similarity in terms of their spatial orientation and process of generation with a previous study by Baj & Buxton (2017) involving a different multiscale geometry. These secondary structures are produced due to interaction between the wakes of different wake generating bodies. Hence, unlike the primary coherent motions (*i.e.* the modes associated with the vortex shedding of the individual wake generating bodies), that are energised by the mean flow, the secondary coherent modes are energised by the non-linear traidic interaction term. In fact we find that most of the energy gained by the secondary coherent motions comes from the high frequency primary mode forming a triad with the secondary modes.

This work raises the question of whether these energy transfers are universal in any complex multiscale flow such as a wind turbine wake. Indeed, non-linear triadic interaction between different coherent structures such as the tip vortices and vortex shedding from the nacelle/tower can excite new structures in a wind turbine wake which might have a significant influence on the spatio-temporal evolution of the wake. Indeed we show that the interaction between the vortices shed from the tower and the tip vortices makes the wake in FOV 2 look totally different from that observed in FOV 1. A number of new frequencies are observed apart from that associated with the shedding of the individual wake generating bodies. Future work will focus on the origin of these new frequencies using the triple decomposed coherent energy budget equations discussed previously. Unlike the multiscale system consisting of a cylinder and a control rod, a wind turbine wake is significantly more complicated due to the flow being highly three dimensional and the presence of rotation. High quality stereoscopic/tomographic PIV experiments are necessary to avail all the terms in the energy budget equations. If the universality of energy exchanges is upheld even for such a complicated system, this will offer a promising strategy to improve the modelling of wind turbine wakes.

REFERENCES

Baj, Pawel, Bruce, Paul JK & Buxton, Oliver RH 2015 The triple decomposition of a fluctuating velocity field in a multiscale flow. *Physics of Fluids* **27** (7), 075104.

Baj, Pawel & Buxton, Oliver RH 2017 Interscale energy transfer in the merger of wakes of a multiscale array of rectangular cylinders. *Physical Review Fluids* **2** (11), 114607.

Biswas, Neelakash, Cicolin, Murilo M & Buxton, Oliver RH 2022 Energy exchanges in the flow past a cylinder with a leeward control rod. *Journal of Fluid Mechanics* **941**.

Cantwell, Brian & Coles, Donald 1983 An experimental study of entrainment and transport in the turbulent near wake of a circular cylinder. *Journal of Fluid Mechanics* **136**, 321–374.

Chamorro, Leonardo P & Porté-Agel, Fernando 2009 A wind-tunnel investigation of wind-turbine wakes: boundary-layer turbulence effects. *Boundary-Layer Meteorology* **132** (1), 129–149.

Cicolin, MM, Buxton, ORH, Assi, GRS & Bearman, PW 2021 The role of separation on the forces acting on a circular cylinder with a control rod. *Journal of Fluid Mechanics* **915**.

Foti, Daniel, Yang, Xiaolei, Campagnolo, Filippo, Maniaci, David & Sotiropoulos, Fotis 2018 Wake meandering of a model wind turbine operating in two different regimes. *Physical Review Fluids* **3** (5), 054607.

Hussain, AKM Fazle 1986 Coherent structures and turbulence. *Journal of Fluid Mechanics* **173**, 303–356.

Okulov, ValeryL, Naumov, IgorV, Mikkelsen, RobertF, Kabardin, IvanK & Sørensen, JensN 2014 A regular strouhal number for large-scale instability in the far wake of a rotor. *Journal of Fluid Mechanics* **747**, 369.

Reynolds, WC & Hussain, AKMF 1972 The mechanics of an organized wave in turbulent shear flow. Part 3. Theoretical models and comparisons with experiments. *Journal of Fluid Mechanics* **54** (2), 263–288.

Rigas, G, Oxlade, AR, Morgans, AS & Morrison, JF 2014 Low-dimensional dynamics of a turbulent axisymmetric wake. *Journal of Fluid Mechanics* **755**.

Schmid, Peter J 2010 Dynamic mode decomposition of numerical and experimental data. *Journal of Fluid Mechanics* **656**, 5–28.

Wynn, Andrew, Pearson, DS, Ganapathisubramani, Bharathram & Goulart, Paul J 2013 Optimal mode decomposition for unsteady flows. *Journal of Fluid Mechanics* **733**, 473–503.